Enhanced thermoelectric properties of W and Fe substituted $MnSi_\gamma$

Swapnil Ghodke[1], Naoya Hiroishi[1], Akio Yamamoto[2], Hiroshi Ikuta[1], Masaharu Matsunami[2], Tsunehiro Takeuchi[2,3,4]

[1]Department of Crystalline Materials Science, Nagoya University, Nagoya, Japan
[2]Toyota Technological Institute, Nagoya, Japan
[3]PRESTO, JST, Tokyo, Japan
[4]GREMO, Nagoya, Japan
E-mail : swapnil@iku.xtal.nagoya-u.ac.jp

Abstract

We have investigated, the effect of heavy element (W) substitution on thermoelectric properties of higher manganese silicide (HMS). Samples were prepared by arc melting followed by liquid quenching, where the latter assisted in achieving higher solubility for tungsten. We observed that the $Mn_{34.6}W_{1.8}Si_{63.6}$ was a p-type material, whereas simultaneous substitution of 12 at.% Fe makes higher manganese silicide a n-type material. The optimal carrier concentration was obtained by simultaneous substitution of Fe and W for Mn atoms. Although the samples were metastable, we have successfully obtained bulk samples by low temperature (970K), high pressure (>100MPa), and long duration sintering process. The lattice thermal conductivity has been effectively reduced by W substitution, and the *ZT* value was improved more than 0.5 for both n-type and p-type samples.

Keywords: Thermoelectric materials, metastable, liquid quenching, sintered bulk

Introduction

The non-renewable fossil fuels in the form of crude oil, coal, or natural gas are being used to fulfill the energy need of our modern society. The electrical energy comes with a cost for industrial as well as household usage. Considering the limited efficiency of energy generation and utilization, we need to utilize the waste heat that is currently given out to the atmosphere. Here, thermoelectric generators (TEG's) are believed to play a key role to convert the waste form of heat energy into useful electrical energy.

The performance of thermoelectric generator is measured by dimensionless figure of merit ($ZT = S^2\sigma T / (\kappa_e+\kappa_l)$), because the efficiency of energy conversion in a thermoelectric generator is an increasing function of ZT. [1] Here, S, σ, κ_e, κ_l, and T represent Seebeck coefficient or thermopower, electrical conductivity, electron thermal conductivity, lattice thermal conductivity, and absolute temperature, respectively. To obtain a high ZT value, we have to find out materials that possess high power factor $S^2\sigma$ together with the low magnitude of thermal conductivity, both from electron and lattice. Theoretically, all the physical quantities are closely coupled to one another, that makes it more challenging to obtain the most efficient thermoelectric material. [1-3] We have to mention, also that many of practical thermoelectric materials possessing high ZT contain expensive and toxic elements such as Lead, Selenium, Antimony, and Tellurium. These elements limit the access and usage of this technology for general applications.

One of the most promising alternative material containing cheap and non-toxic elements, while possessing a large magnitude of ZT is higher manganese silicide stabilized at $MnSi_\gamma$ ($1.73 \leq \gamma \leq 1.75$). The thermal and mechanical stability of HMS at high temperature gives the capability to work in operational temperature range of 600 – 800 K. [1,4] The p-type HMS have shown large Seebeck coefficient ~ $220\mu VK^{-1}$, low electrical resistivity ~ $2x10^{-3}\Omega cm$, and thermal conductivity ~ 2.5 WmK^{-1} with maximum ZT of ~0.5 at 800 K. [5,6]

Unfortunately, the *ZT*-value is not competitive with the commercially available thermoelectric materials. The need to improve the performance of higher manganese silicide has drawn our attention to investigate a new technique that can enhance the *ZT*. Recently, Takeuchi *et al.* [7,8] have reported a guiding principle for increasing the performance of thermoelectric materials by reducing lattice thermal conductivity without altering electron transport properties. Here, the lattice thermal conductivity was greatly reduced by substitution of heavy elements especially when the material is consisting solely of light elements such as the present Mn-Si. While the electron transport properties are hardly affected by it, partly because of the system that stays in the strongest scattering limit have a very weak temperature dependence of electrical resistivity, provided that any impurity states are produced in the electronic structure near the chemical potential by the element substitution.

It is also essential for the practical thermoelectric generator to have both n-type and p-type material of similar composition because of thermal expansion and mechanical properties. Both n-type and p-type HMS's were reported to be successfully prepared, but, unfortunately, the value of *ZT* observed for an n-type sample was much smaller than that of p-type samples.[9] Therefore, we also need to develop n-type HMS for making practical thermoelectric generators.

In this study, we focused on preparing cheapest and most efficient higher manganese silicide compound for the thermoelectric generator by introducing heavy tungsten atoms as the substitute for manganese atoms. We selected tungsten partly because it was used for the partial substitution for manganese in Si_2Ti-type Al-Mn-Si, which has the similar local atomic arrangement with that of HMS, and partly because it is non-toxic and the cheapest element among the all 5d transition metal elements. Considering the negligibly small solubility of W in higher manganese silicide,[10] we have used rapid quenching technique to increase the solubility limit of W. Besides, to find out the optimal carrier concentration both for p-type and n-type, we have simultaneously employed Fe substitution for Mn.

Experimental procedure:

Samples with $Mn_{36.4-x}W_xSi_{63.6}$ ($0 \leq x \leq 7.3$) and $Mn_{36.4-x-y}W_xFe_ySi_{63.6}$ (x = 1.8 or 3.6, $0 \leq y \leq 14.4$) composition were obtained by mixing manganese (99.99%), silicon (99.99%), tungsten (99.99%), and iron (99.99%) powders by using mortar and pestle and compacted into pellets. The pellets are melted in arc furnace under pressurized argon atmosphere for several times to obtain a homogeneous ingot. We also employed single role liquid quenching technique, where the ingot was re-melted in the silica tube and injected on a copper wheel rotating at 4500 rpm in Argon atmosphere. The ribbon-shaped samples were obtained with 10~15 mm in length, 0.5~0.1 mm in width, and 10~15 μm in thickness. The ribbons were grounded into powder by using mortar and pestle. The obtained powders were sintered in a graphite die (ϕ10 mm) by spark plasma sintering under ~100 MPa at 950 K for 150 min in vacuum atmosphere.

In this study, we have investigated the thermoelectric properties both for the liquid quenched ribbons and the bulk-sintered samples. The phases involved in the samples were identified by powder X-ray diffractometer of BRUKER D8 Advance with Cu-Kα radiation. Seebeck coefficient was measured by steady state method using Seebeck Measurement System manufactured by Micro-Miniature Refrigerator (MMR) Technologies, inc. Electrical resistivity was measured using four probe method. Thermal conductivity was calculated by formula $\kappa = D\rho C_V$, thermal diffusivity (D) was measured by laser flash technique (LFA457, NETZSCH), heat capacity (C_V) by using differential scanning calorimetry (DSC 8231, RIGAKU), and the density (ρ) of sintered samples by Archimedes method.

Results

The measured X-ray diffraction (XRD) patterns of $Mn_{36.36-x}W_xSi_{63.64}$ ($0 \leq x \leq 7.3$) are plotted in Fig.1 (a) and Fig.1 (b) for arc-melted samples and liquid quenched samples, respectively. The XRD pattern of arc-melted samples clearly shows peaks of impurity phases (Si_2W and MnSi) even with a very small amount of W, on the contrary, the impurity peaks disappears for x = 1.8 and x = 3.6 after liquid quenching. In Fig.1 (c), lattice

constant calculated from the XRD data of liquid quenched samples monotonically increases with increasing W concentration at $x \leq 3.6$, but became almost constant at $3.6 \leq x \leq 7.3$. These data clearly indicate the solubility limit is at least 3.6 at.%W in higher manganese silicide.

After successfully obtaining the solid solution with W, the carrier concentration was controlled by additionally substituting Fe for Mn. The solubility limit of Fe in HMS was found to reach up to 15 at.%, which can be clearly confirmed from the XRD patterns shown in Fig. 2 (a) and (b). Miyazaki *et al.* reported that the solubility limit of Fe in HMS was less than 10 at.%.[9] The increase of Fe concentration would be caused in association with the simultaneously introduced W, this is similar to results obtained for the double doped (Al, Fe) HMS solid solution, where the solubility limit of Al was increased by Fe substitution.[11] The large amount of Fe in HMS naturally leads to a larger number of electron concentration, and which can be used as an n-type material.

Thermoelectric properties of liquid quenched and bulk samples were investigated. Seebeck coefficient at room temperature is plotted as a function of Fe concentration in Fig. 3 (a). All the three series of samples, $Mn_{34.6-y}W_{1.8}Fe_ySi_{63.6}$ ($0 \leq y \leq 14.4$), $Mn_{32.8-y}W_{3.6}Fe_ySi_{63.6}$ ($0 \leq y \leq 14.4$), and $Mn_{36.4-y}Fe_ySi_{63.6}$,[9] show similar behavior irrespective of different W content. This fact indicates that tungsten atom does not produce any impurity states near the chemical potential when it is located in Mn-site in HMS. The sign of Seebeck coefficient was positive at $y \leq 10$ while it turned out to be negative at $y \geq 10$. The magnitude of electrical resistivity divergently increased near the compositions where Seebeck coefficient had shown transition. These facts are well interpreted for the presence of energy gap between the valence and conduction bands together with the shift of Fermi energy by varying Fe concentration. Fig. 3 (c) shows composition dependence of power factor. The maximum power factor for p-type $Mn_{34.56}W_{1.8}Si_{63.64}$ $0.7mWm^{-1}K^{-2}$ and for n-type $Mn_{18.36}W_{3.6}Fe_{14.4}Si_{63.6}$ $0.46mWm^{-1}K^{-2}$ was obtained at 300K.

The ribbon samples prepared in this study were thermodynamically metastable and therefore investigated

the thermal stability by Differential Thermal Analysis (DTA). As a typical example, we have shown the DTA curve observed for $Mn_{32.76}W_{3.6}Si_{63.64}$ in Fig. 4 (a). A sharp exothermic peak was observed at around 1000 K, presumably indicating the phase transition from metastable HMS to a mixed phase of HMS and other. The Fig.4 (b) shows XRD pattern of a sample heat treated above 1000K, which clearly shows secondary phases. The working temperature of HMS is supposed to be lower than 900 K because it possesses the largest value typically at around 800 K.[9] These facts let us firmly believe that the thermal stability of the metastable HMS containing a small amount of W is good enough for making bulk samples.

The sintering temperature for HMS, however, was reported to be 1223 K, which is much higher than the decomposing temperature. Therefore, we tried to employ a high pressure (100 MPa), and long duration (150min) pulse current sintering process at 973K. As a consequence, the bulk samples having 90 % of theoretical density was successfully prepared for p-type $Mn_{32.6}W_{1.8}Si_{63.6}$ and n-type $Mn_{18.4}W_{3.6}Fe_{14.4}Si_{63.6}$. In Fig.4 (b) the XRD pattern shows almost no phase separation for the sintered sample. Although the density was slightly smaller than the ordinary samples, we decided to study the thermoelectric properties of these slightly porous samples.

Fig. 5 shows the temperature-dependent thermoelectric properties of prepared bulk samples. We should note that the Seebeck coefficient of the present p-type $Mn_{32.56}W_{1.8}Si_{63.64}$ shows almost the same magnitude and temperature dependence with those of $Mn_{36.36}Si_{63.64}$ most likely due to the absence of impurity states near the chemical potential in association with tungsten atoms. The electrical resistivity of p-type $Mn_{34.6}W_{1.8}Si_{63.6}$ shows slightly larger value than that of p-type $Mn_{36.4}Si_{63.6}$ mainly due to the lower density. The thermal conductivity of p-type $Mn_{34.6}W_{1.8}Si_{63.6}$ also showed a lower value than that of $Mn_{36.36}Si_{63.64}$ due to the low density and phonon scattering effect of W. As a result, the magnitude of *ZT* was increased by 10 % for p-type $Mn_{32.56}W_{1.8}Si_{63.64}$ from that of p-type $Mn_{36.36}Si_{63.64}$. The largest *ZT* value reached up to 0.5 at 700 K, and this value is supposed to increase at around 800 K although we did not confirm it because of the experimental limitation.

Notably, n-type $Mn_{18.4}W_{3.6}Fe_{14.4}Si_{63.6}$ also shows almost the same magnitude of *ZT* with that of p-type $Mn_{32.6}W_{1.8}Si_{63.6}$, which is the largest value ever observed for n-type HMS. This result together with the non-toxic, less-expensive characteristics strongly let us believe that the HMS could become practical thermoelectric material widely used for various applications.

Discussion

The magnitude of *ZT* observed for the present HMS containing a small amount of tungsten was much less than unity, and was presumably inappropriate for practical applications. We should comment, however, that we have still chance to increase the *ZT*-value by using other 5d transition metal elements. For example, we succeeded in increasing *ZT* of Si_2Ti-type Al-Mn-Si alloys by employing Ru and Re substitutions for Mn. [12] This method with tungsten atoms was also applied for $CrSi_2$-type Al-Mn-Si alloys. [13] The lattice thermal conductivity of these alloys was drastically decreased with increasing heavy element concentrations. The similarity in local atomic arrangements between Si_2Ti-type structure, Cr_2Si-type structure, and HMS suggests that by substituting 5d elements in HMS can effectively reduce lattice thermal conductivity. Recent reports on Re substitution for Mn in HMS confirms the reduction in lattice thermal conductivity. [14, 15]

Another method to improve *ZT*-value is nanostructure formation. If we could prepare nanostructures, such as superlattice or quantum wells, the lattice thermal conductivity would be further reduced to increase the *ZT*-value of HMS effectively.

Recently, we have also tried to increase the *ZT* value of HMS by using energy filtering effect.[16] This effect was experimentally confirmed in association with the grain boundary scattering. The samples with very fine grains would lead to an increase of Seebeck coefficient and reduction of lattice thermal conductivity to increase *ZT*.

The methods mentioned above are now under investigation in our group, and the results will be presented in near future elsewhere.

Conclusion

In this study, we have tried to improve the performance of HMS by simultaneously substituting W and Fe for Mn. The rapid cooling by single role liquid quenching technique effectively increased the solubility limit of W in HMS up to 3.6 at%. The simultaneous substitution of Fe and W for Mn has helped in obtaining both n-type and p-type samples. We have successfully prepared bulk samples by using low temperature (950 K), high pressure (100 MPa) and long sintering (150 min.) technique below phase transition temperature, which was not possible by using conventional sintering parameter used for HMS. The W substitution has effectively reduced the thermal conductivity without affecting the electronic structure, which leads to improvement in the magnitude of *ZT*. The maximum *ZT* value obtained for both n- and p-type samples was 0.5 at 700K.

Acknowledgement

This work was conducted under the financial support of JST PRESTO and Japan Society for the Promotion of Science (JSPS) KAKENHI, Grant Nos. 26289236 and 26630332.

References

[1] H. J Goldsmid, CRC Handbook of Thermoelectrics ed. by D. M. Rowe (CRC Press, Boca Raton, 1995), pp. 22-23.

[2] H. J. Goldsmid, Introduction to Thermoelectricity, (Springer, Heidelberg, 2009), pp. 43-61.

[3] J. R. Sootsman, D.Y. Chung, M.G. Kanatzidis: Angew. *Chem. Int. Ed. Engl*. **48** (2009) 8616–8639.

[4] Yuzuru Miyazaki and Yuta Kikuchi, Thermoelectric Nanomaterials, ed. by K. Koumoto and T. Mori (Springer, Heidelberg, 2013) Vol. 182, pp.141-155.

[5] Y. Kikuchi, Y. Miyazaki, Y. Saito, K. Hayashi, K. Yubuta, T. Kajitani, *Jpn. J. Appl. Phys.* **51**, (2012) 085801. doi:10.1143/JJAP.51.085801

[6] T. Itoh, and M. Yamada, *J. Electron. Mater.***38,** 925-929. (2009)

[7] M. Mikami , Y. Kinemuchi, K. Ozaki, Y. Terazawa, T. Takeuchi., *J. Appl. Phys.* **111**, 093710. (2012) doi: 10.1063/1.4710990

[8] T. Takeuchi, Y. Terazawa, Y. Furuta, A. Yamamoto, M. Mikami. *J. Electron. Mater.* **42**, 2084-2090. (2013)

[9] Y. Miyazaki, Y. Saito, K. Hayashi, K. Yubuta, T. Kajitani: *J. Appl. Phys.* **50** 035804. (2011) doi: 10.7567/JJAP.50.035804

[10] P. Villars, A. Prince, H. Okamoto, Handbook of ternary alloy phase diagram, (ASM International, Ohio, 1995) Vol. **10**, p. 12463.

[11] S.A. Barczak, R.A. Downie, S. R. Popuri, R. Decourt, M. Pollet, J. W. G. Bos, *J. Solid State Chem*, **227**, 55–59. (2015) doi: 10.1016/j.jssc.2015.03.017

[12] A. Yamamoto, H. Miyazaki,T. Takeuchi, *J. Appl. Phys.* **115**, 023708.(2014) doi:10.1063/1.4861643

[13] A. Yamamoto, H. Miyazaki, M. Inukai, Y. Nishino, T. Takeuchi: *Jpn. J. Appl. Phys.* 071801. (2015) doi:10.7567/JJAP.54.071801

[14] X. Chen, S. N. Girard, F. Meng, E. Lara-Curzio, S. Jin, J.B. Goodenough, J. Zhou, L. Shi , *Adv. Energy*

Mater. 4, 1400452. (2014) doi: 10.1002/aenm.201400452

[15] A. Yamamoto, S. Ghodke, H. Miyazaki, M. Inukai, Y. Nishino, M. Matsunami, and T. Takeuchi, *J. Appl. Phys* **55**, 020301. (2016) doi:10.7567/JJAP.55.020301

[16] S. Ghodke, A. Yamamoto, H. Ikuta, T. Takeuchi: Proceedings. of *11th International Conference on Ceramic Materials and Components for Energy and Environmental Applications, American ceramic society*, 14-20 June 2015, Vancouver, Canada.

Figure captions

Figure 1 XRD data plotted of (a) arc-melted and (b) Liquid-quenched $Mn_{36.4-x}W_xSi_{63.6}$. Lattice constant *a* is plotted as a function of W concentration in (c).

Figure 2 XRD data plotted of liquid-quenched (a) $Mn_{34.6-y}W_{1.8}Fe_ySi_{63.6}$ and (b) $Mn_{32.8-y}W_{3.6}Fe_ySi_{63.6}$ Lattice constants *a* and *c* are plotted as a function of W concentration in (c) and (d) for $Mn_{34.6-y}W_{1.8}Fe_ySi_{63.6}$ and $Mn_{32.8-y}W_{3.6}Fe_ySi_{63.6}$, respectively.

Figure 3 (a) Electrical resistivity, (b) electrical resistivity, and (c) of $Mn_{36.6-y}Fe_ySi_{63.4}$,[REF9] $Mn_{34.6-y}W_{1.8}Fe_ySi_{63.6}$, and $Mn_{32.8-y}W_{3.6}Fe_ySi_{63.6}$ plotted as a function of Fe concentration.

Figure 4 (a) DTA curve of liquid quenched $Mn_{32.8}W_{3.6}Si_{63.4}$ and (b) XRD patterns measured after liquid-quenching, heat treatment at 1100 K and sintering at 973K.

Figure 5 (a) Seebeck coefficient, (b) electrical resistivity, (c) thermal conductivity, and (d) dimensionless figure of merit observed for p-type $Mn_{34.6}W_{1.8}Si_{63.6}$ and n-type $Mn_{18.4}W_{3.6}Fe_{14.4}Si_{63.6}$ bulk samples.

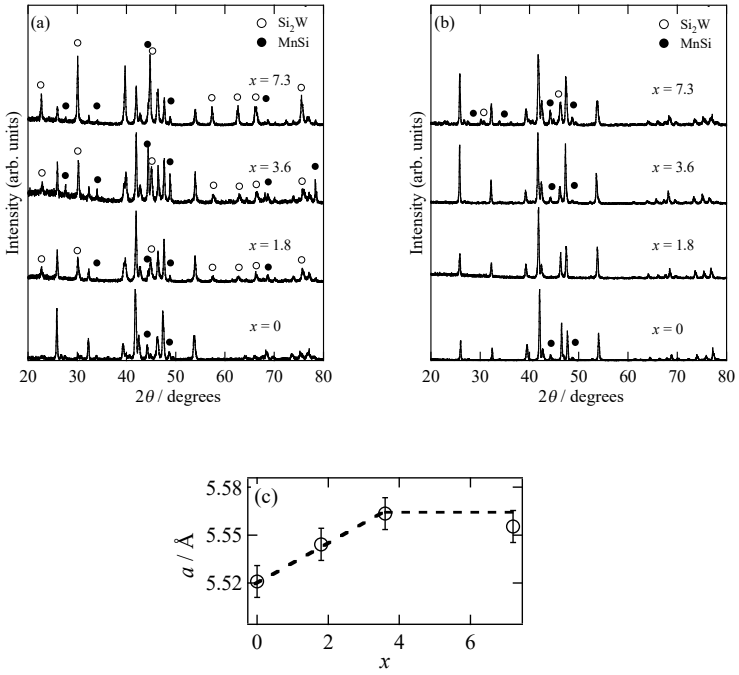

Figure 1 XRD data plotted of (a) arc-melted and (b) Liquid-quenched $Mn_{36.4-x}W_xSi_{63.6}$. Lattice constant *a* is plotted as a function of W concentration in (c).

Figure 1 *Ghodke et al.*

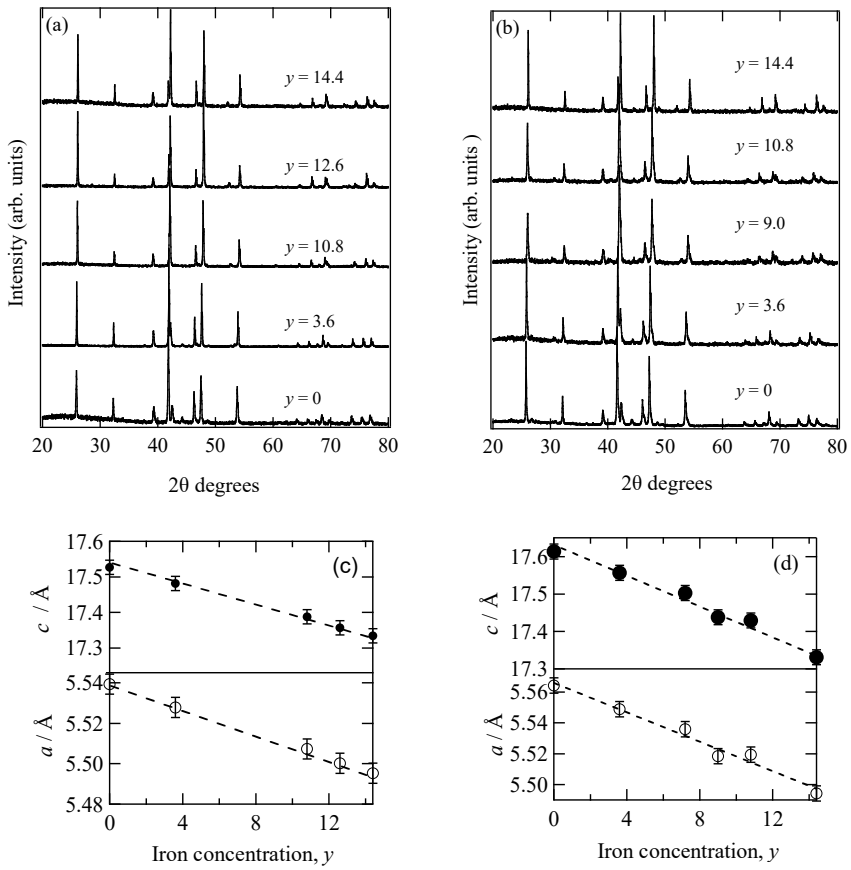

Figure 2 XRD data plotted of liquid-quenched (a) $Mn_{34.6-y}W_{1.8}Fe_ySi_{63.6}$ and (b) $Mn_{32.8-y}W_{3.6}Fe_ySi_{63.6}$ Lattice constants *a* and *c* are plotted as a function of W concentration in (c) and (d) for $Mn_{34.6-y}W_{1.8}Fe_ySi_{63.6}$ and $Mn_{32.8-y}W_{3.6}Fe_ySi_{63.6}$, respectively.

Figure 2 *Ghodke et al.*

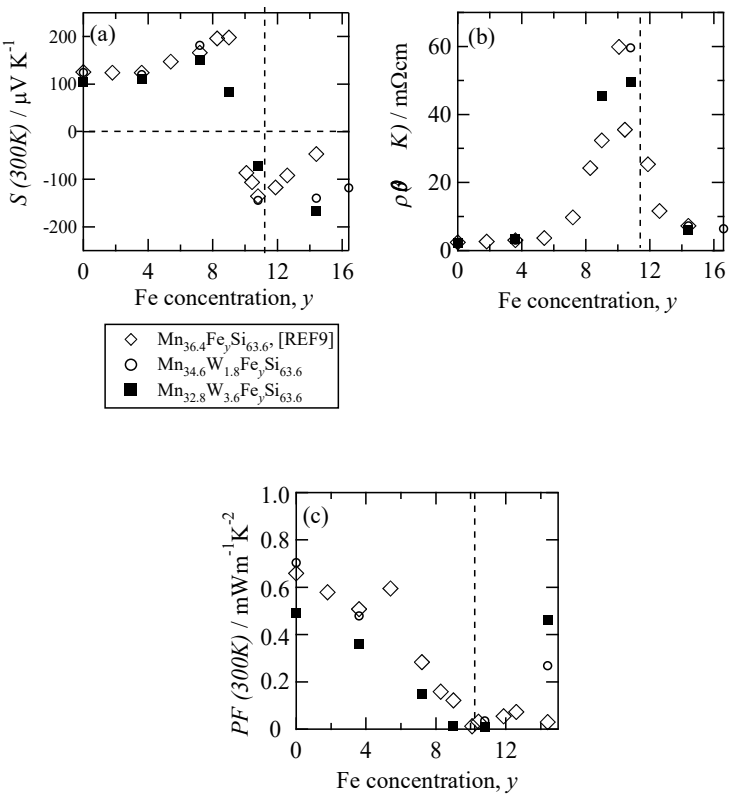

Figure 3 (a) Electrical resistivity, (b) electrical resistivity, and (c) of $Mn_{36.6-y}Fe_ySi_{63.4}$,[REF9] $Mn_{34.6-y}W_{1.8}Fe_ySi_{63.6}$, and $Mn_{32.8-y}W_{3.6}Fe_ySi_{63.6}$ plotted as a function of Fe concentration.

Figure 3 *Ghodke et al.*

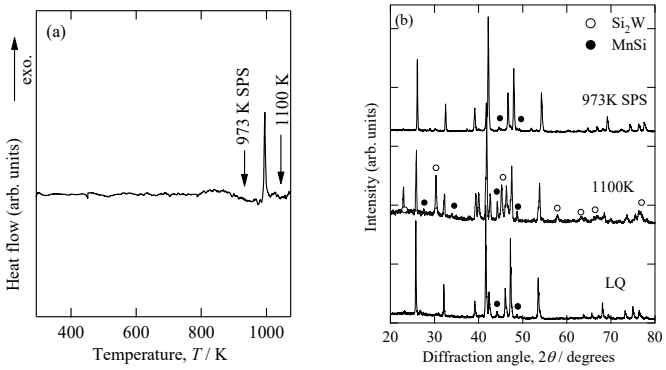

Figure 4 (a) DTA curve of liquid quenched $Mn_{32.8}W_{3.6}Si_{63.4}$ and (b) XRD patterns measured after liquid -quenching, heat treatment at 1100 K and sintering at 973K.

Figure 4 *Ghodke et al.*

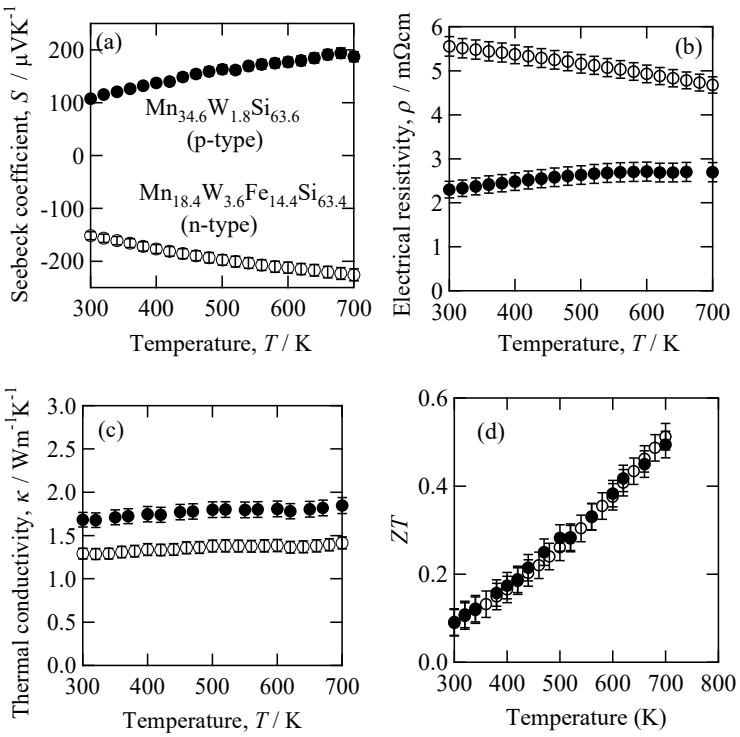

Figure 5 (a) Seebeck coefficient, (b) electrical resistivity, (c) thermal conductivity, and (d) dimensionless figure of merit observed for p-type $Mn_{34.6}W_{1.8}Si_{63.6}$ and n-type $Mn_{18.4}W_{3.6}Fe_{14.4}Si_{63.6}$ bulk samples.

Figure 5 *Ghodke et al.*